ARL-TR-9057 ● SEP 2020


# Density Functional Theory Study of Σ9 {122} Grain Boundaries in Silicon and Silicon Carbide-3C

by Jennifer Synowczynski-Dunn, Matthew Guziewski, and Shawn Coleman

## NOTICES

### Disclaimers

The findings in this report are not to be construed as an official Department of the Army position unless so designated by other authorized documents.

Citation of manufacturer's or trade names does not constitute an official endorsement or approval of the use thereof.

Destroy this report when it is no longer needed. Do not return it to the originator.

ARL-TR-9057 ● SEP 2020


# Density Functional Theory Study of Σ9 {122} Grain Boundaries in Silicon and Silicon Carbide-3C

**Jennifer Synowczynski-Dunn, Matthew Guziewski, and Shawn Coleman**
***Weapons and Materials Research Directorate, CCDC Army Research Laboratory***

# REPORT DOCUMENTATION PAGE

*Form Approved*
*OMB No. 0704-0188*



| 1. REPORT DATE *(DD-MM-YYYY)* | 2. REPORT TYPE | 3. DATES COVERED (From - To) |
|---|---|---|
| September 2020 | Technical Report | 1 January–1 October 2019 |

**4. TITLE AND SUBTITLE**
Density Functional Theory Study of Σ9 {122} Grain Boundaries in Silicon and Silicon Carbide-3C

**5a. CONTRACT NUMBER**

**5b. GRANT NUMBER**

**5c. PROGRAM ELEMENT NUMBER**

**6. AUTHOR(S)**
Jennifer Synowczynski-Dunn, Matthew Guziewski, and Shawn Coleman

**5d. PROJECT NUMBER**

**5e. TASK NUMBER**

**5f. WORK UNIT NUMBER**

**7. PERFORMING ORGANIZATION NAME(S) AND ADDRESS(ES)**
CCDC Army Research Laboratory
ATTN: FCDD-RLW-ME
Aberdeen Proving Ground, MD 21005

**8. PERFORMING ORGANIZATION REPORT NUMBER**
ARL-TR-9057

**9. SPONSORING/MONITORING AGENCY NAME(S) AND ADDRESS(ES)**

**10. SPONSOR/MONITOR'S ACRONYM(S)**

**11. SPONSOR/MONITOR'S REPORT NUMBER(S)**

**12. DISTRIBUTION/AVAILABILITY STATEMENT**
Approved for public release; distribution is unlimited.

**13. SUPPLEMENTARY NOTES**
ORCID IDs: Shawn Coleman, 0000-0002-5542-3161; Matthew Guziewski, 0000-0002-5761-720X

**14. ABSTRACT**
In this report, we perform a first-principles density functional theory (DFT) study of the interfacial energies and electronic structure of the Σ9 {122} tilt grain boundary in silicon carbide (SiC)-3C and Si. In SiC-3C, there are three unique reconstructions of this grain boundary: nonpolar, polar C-rich, and polar Si-rich. DFT calculations determined the interfacial energy for the Σ9 {122} silicon, Σ9 {122} SiC-3C nonpolar, and Σ9 {122} SiC-3C polar interfaces are 0.1821, 1.346, and 1.336 J/m$^2$, respectively, indicating the polar interface is more stable in SiC-3C. However, due to periodic boundary conditions, the interfacial energy calculated for the polar interface is an average of the two unique polar Si-rich and C-rich interfaces, whereas the nonpolar interface is symmetric within the supercell. In addition, a detailed analysis of the electronic structure including the electron density difference, Mulliken charge transfer, and atom-resolved partial density of states within the grain boundary region was performed to determine how electron redistribution and interfacial reconstruction affects local chemical reactivity.

**15. SUBJECT TERMS**
SiC, grain boundary, DFT, electronic structure, interfacial reconstruction

| 16. SECURITY CLASSIFICATION OF: | | | 17. LIMITATION OF ABSTRACT | 18. NUMBER OF PAGES | 19a. NAME OF RESPONSIBLE PERSON |
|---|---|---|---|---|---|
| a. REPORT | b. ABSTRACT | c. THIS PAGE | | | Jennifer Dunn |
| Unclassified | Unclassified | Unclassified | UU | 21 | 19b. TELEPHONE NUMBER (Include area code) (410) 306-0750 |

## Contents

## List of Figures



## List of Tables

## Acknowledgments

This research was sponsored by the Department of Defense High Performance Computing Modernization Program (HPCMP).

## 1. Introduction

Silicon carbide (SiC) is currently the ceramic of choice for lightweight ultra-hard armor ceramics due to its low density (~3 g/cm$^3$), high hardness (HV ~22 GPa),[1] and high elastic modulus ($E$ = 400–420 GPa),[1] which results in a competitive ballistic energy dissipation criterion $D$ of 4.4 × $10^{-12}$/s.[2] However, the ballistic performance of SiC could be significantly improved if its fracture resistance under dynamic transient loading $K_{ic\text{-}dynamic}$ is increased while maintaining high hardness. The fracture toughness is highly dependent on the properties of the grain boundaries for monolithic ceramics. For example, during transgranular fracture (i.e., grain boundaries are stronger than the bulk crystal), the fracture toughness of SiC is limited to approximately 2–3 MPa•m$^{1/2}$ whereas during intergranular fracture (i.e., grain boundaries are weaker than bulk crystal) $K_{ic}$ can approach 10 MPa•m$^{1/2}$.[3]

The most frequently observed grain boundaries in polycrystalline silicon-based ceramics are the Σ3{111} and Σ9 {122} tilt boundaries,[4] which form triple junctions in silicon,[5] geramanium,[6] diamond,[7] and silicon carbide.[8] The goal of this research study is to provide process engineers with the chemical intuition necessary to promote intergranular fracture in SiC-3C by developing a first-principles density functional theory (DFT) model for the relationship between electronic structure, interfacial grain boundary reconstruction, local chemical activity, and bond strength for the Σ9 {122} tilt grain boundary in SiC-3C and silicon.

## 2. Structure of the Σ9 {122} Tilt Boundary

The Σ9 {122} SiC-3C tilt grain boundaries within this study were created by introducing edge dislocations into the SiC lattice, consistent with the zigzag model from Kohyama.[8] This grain boundary has a tilt angle of 39.94°. The grain boundary interface is composed of two repeating structural units, each consisting of one five- and seven-membered ring. Fig. 1b, c, d, and e correspond to the edge dislocations shown in Figure 15a, b, c, and d, respectively, from Kohler.[9] Because there is an odd number of atoms in each ring, one of the bonds within the ring is between like atoms, hereafter referred to as “wrong bonding” because it is inconsistent with the SiC-3C bulk bonding. There are three unique arrangements of the structural units within the Σ9 {122} SiC-3C tilt grain boundary (Fig. 2): 1) nonpolar interface, composed of structural units (Fig. 1d and e) with alternating C-C and Si-Si bonds, 2) polar C-rich interface, composed entirely of structural units (Fig. 1b) containing C-C bonds, and 3) polar Si-rich interface, composed entirely of structural units (Fig. 1c) containing Si-Si bonds.

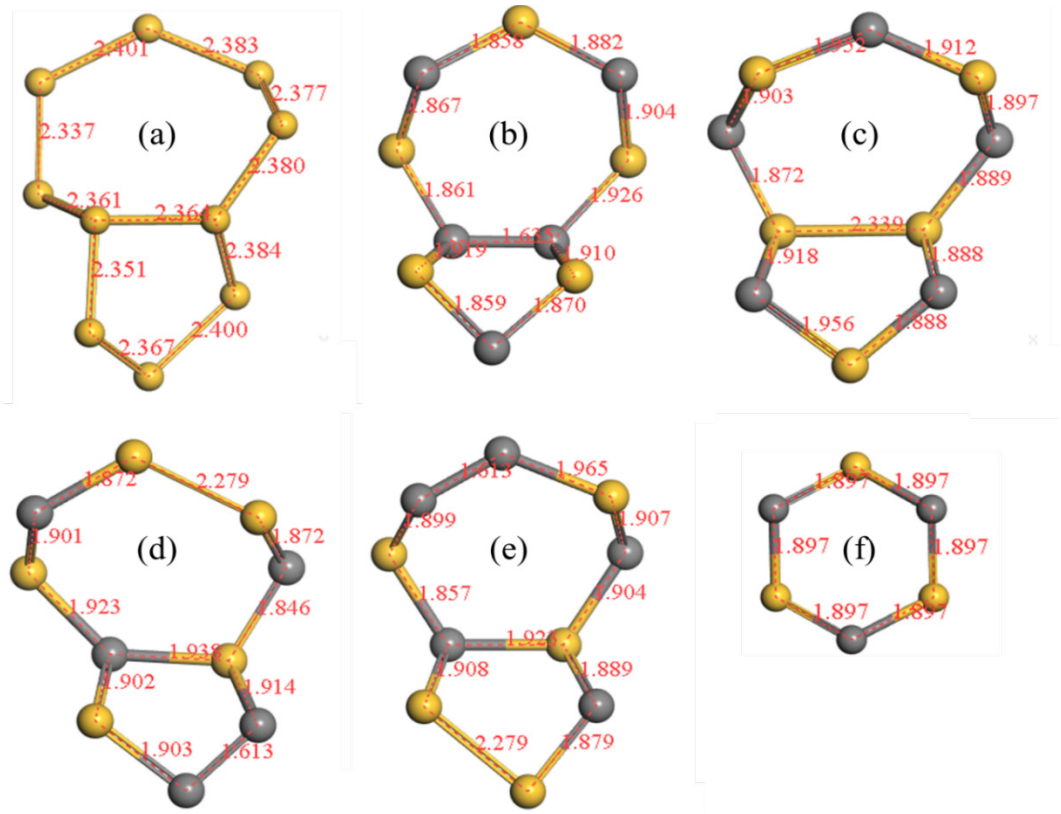


**Fig. 1 Structural units showing bond lengths (Å) for a) Σ9 {122} silicon tilt boundary, b) Σ9 {122} SiC-3C polar C-rich, c) Σ9 {122} SiC-3C polar Si-rich, d) Σ9 {122} SiC-3C nonpolar unit 1, e) Σ9 {122} SiC-3C nonpolar unit 2, and f) bulk SiC-3C. Note: for this figure and all subsequent figures, carbon atoms are grey and silicon atoms are gold.**

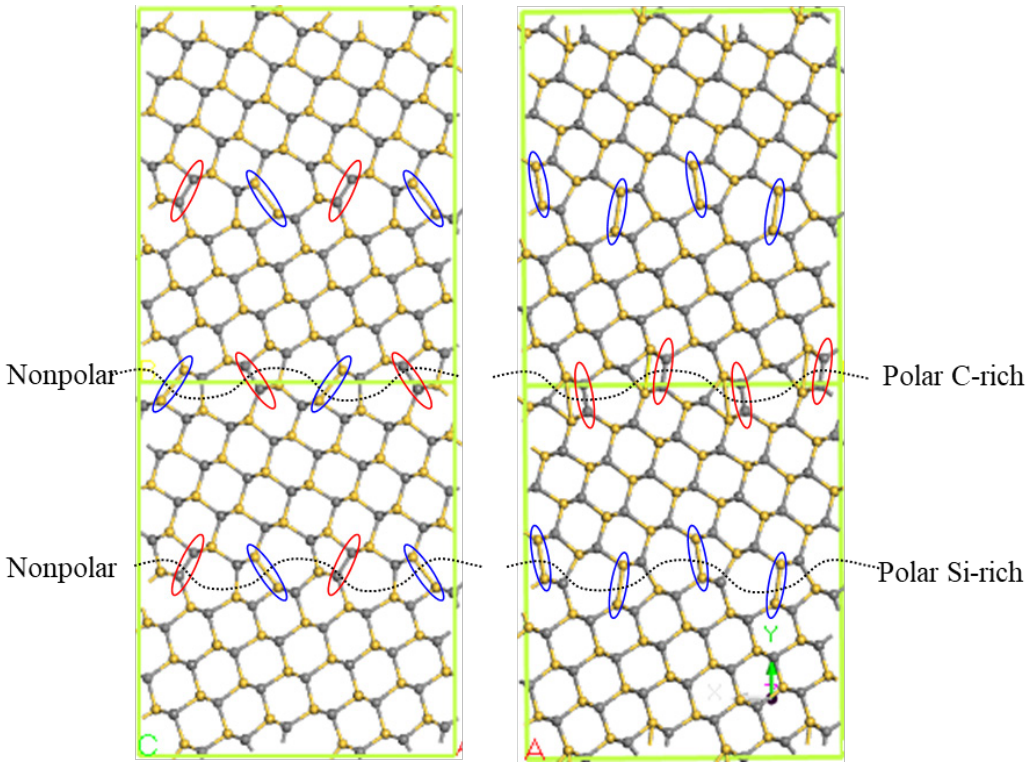


**Fig. 2 Three unique interfaces for the Σ9 {122} SiC-3C tilt grain boundary. Blue and red ellipses highlight the Si-Si and C-C bonding, respectively, along the grain boundary interfaces.**

## 3. Computational Method

The starting structure for the Σ9 {122} SiC-3C tilt grain boundary contains 240 atoms within a rectangular supercell (a = 18.7 Å, b = 34.6 Å, c = 6.2 Å) with the boundary oriented normal to the y-axis. Due to the periodic boundary conditions, each supercell contains two interfaces that are equivalent for the nonpolar grain boundary but distinct for the polar grain boundary. These structures were generated using Monte Carlo[10] and optimized using the SiC.tersoff[11] classical molecular dynamics potential implemented within Large-scale Atomic/Molecular Massively Parallel Simulator, or LAMMPS,[12,13] before being submitted for DFT calculations.

All quantum mechanical calculations were performed within the plane wave (PW) CASTEP DFT code[14] using the Perdew-Burke-Ernzerhoff functional[15] with the generalized gradient approximation (GGA) and a PW cutoff energy equal to 480 eV. The ionic cores were described by ultra-soft pseudopotentials.[16] The calculations were considered converged when the absolute value of the force on each ion was less than or equal to 0.03 eV/Å and the change in the total energy was less than or equal to $10^{-5}$ eV.

The cohesive energy of bulk SiC-3C (–328.6 eV/atom) and silicon (–170.5 eV/atom) was calculated using Eq. 1 where $E_{total}$ is the total system energy for the bulk SiC-3C after full relaxation and $N$ is the number of formula units.

$$E_{coh} = \frac{E_{total}}{N}. \quad (1)$$

The grain boundary energy for the Σ9 {122} SiC-3C tilt was calculated using Eq. 2 where $E_{SiC}$ is the energy per formula unit of SiC as determined from the bulk cohesive energy calculation, and $A$ is the area of the grain boundary. $E_{gb}$ for the polar grain boundary is an average of two unique grain boundary structures due to the asymmetry introduced by the periodic boundary conditions of the supercell.

$$E_{gb} = \frac{E_{total} - [N \cdot E_{SiC}]}{2A} \quad (2)$$

The electron density difference (EDD) maps shown in Section 4.2 are calculated using Eq. 3 where $\rho_{GB}$ is the electron density of the optimized grain boundary and $\rho_i$ is the electron density for the isolated atoms.

$$\Delta\rho = \rho_{GB} - \sum \rho_i. \quad (3)$$

# 4. Simulation Results

## 4.1 Structural Analysis

Bulk SiC-3C has a cubic zinc blende crystal structure (space group $F\bar{4}3m$, no.216; point group $T_d^2$) with an ABCABC stacking along the {111} plane of hexagonal rings composed of tetrahedrally coordinated silicon and carbon. The predicted lattice parameters for the conventional unit cell of SiC-3C and silicon are a = b = c = 4.38 Å and 5.46 Å, respectively, which are in good agreement with the experimentally measured values of 4.3596[17] and 5.43 Å.[18]

The calculated grain boundary energies for the Σ9 {122} silicon, Σ9 {122} SiC-3C nonpolar, and Σ9 {122} SiC-3C polar interfaces are 0.1821, 1.346, and 1.336 J/m$^2$, respectively, which compare well with the values reported by various groups in the literature (Table 1). The grain boundary energy for Σ9 {122} boundaries in silicon is an order of magnitude less than for SiC-3C. This could be explained by the presence of Si-Si and C-C wrong bonds within SiC-3C Σ9 {122} interface that raises the system energy. Although the predicted grain boundary energy for the polar grain boundary is the average of the Si-rich and C-rich interfaces, DFT calculations show that it is more stable than the nonpolar interface and therefore predicted to be slightly more prevalent throughout the SiC-3C microstructure.

**Table 1 Comparison of calculated grain boundary energies for Σ9 {122} SiC-3C nonpolar, Σ9 {122} SiC-3C polar, and Σ9 {122} silicon interfaces to literature**

| Interface | $E_{gb}$ ($J/m^2$) | $E_{gb}$ Literature [Ref] |
|---|---|---|
| SiC Σ9 {122} nonpolar | 1.346 | 1.27 [8]; 1.369 [19]; 1.82 [9] |
| SiC Σ9 {122} polar | 1.336 | $E_{c\text{-}rich}$ = 1.60 $E_{si\text{-}rich}$ = 1.42 [9] |
| Si Σ9 {221} | 0.182 | 0.16 [20]; ~0.18 [5]; 0.183 [21] |

Table 2 lists the bond length and angle distortions for all bonds within the four unique structural units of Σ9 {122} SiC-3C and silicon grain boundaries. All atoms within the grain boundary region are fully coordinated, meaning that there are no dangling bonds in the interfacial region. The creation of 7- and 5-member rings results in large bond angle distortions (7-member ring angle expansion; 5-member ring angle contraction) but minimal bond length distortions (<4% for all Si-C bonds) within the grain boundary region. The largest bond length (BL) and bond angle (BA) distortions occur near the Si-Si (+20 < BL < +23%) and C-C (–15 < BL < –13.8%) wrong bonds. These distortions create periodic compressive (near C-C) and tensile (near Si-Si) strain fields that can serve as gettering sites for dopants. The contraction of the C-C wrong bonds is stronger for the nonpolar interface when compared to the polar C-rich interface, indicating a larger driving force within the nonpolar interface for strain energy minimization via the substitution of carbon atoms by larger atomic species. Conversely, the expansion of the Si-Si wrong bonds is greater for the polar interface when compared to the nonpolar interface. Therefore, the Si-rich polar interface has a higher potential for strain energy minimization when silicon atoms are replaced by dopants with a smaller radius. Since the C-C wrong bonding is only 4.7% larger than bulk diamond C-C bonding, increasing the C-C wrong bonding concentration within the grain boundary region is predicted to reduce the interfacial strain between SiC-3C and diamond. The lattice match is even closer for the Si-Si (–0.6%) wrong bonds in the polar rich Si interface and bulk silicon.

**Table 2 Bond length (BL) and bond angle (BA) distortions for each bond within the silicon Σ9, SiC Σ9 polar-C rich, SiC Σ9 polar-Si rich, and SiC Σ9 nonpolar structural units. Bond numbering system begins at the apex of the fragments shown in Fig. 1 and increments clockwise with bond 11 corresponding to the bond that joins the 7- and 5-member rings. Distortions are calculated with respect to the Si-C bond length and bond angle in bulk SiC-3C. Positive values represent expansion, whereas negative values correspond to compression. Blue and red entries denote C-C and Si-Si wrong bonds, respectively.**

| Bond no. | Silicon Σ9 | | SiC Σ9–C | | SiC Σ9–Si | | SiC Σ9–NP1 | | SiC Σ9–NP2 | |
|---|---|---|---|---|---|---|---|---|---|---|
| | BL (%) | BA (%) | BL (%) | BA (%) | BL (%) | BA (%) | BL (%) | BA (%) | BL (%) | BA (%) |
| 1 | 0.5 | 17.4 | –4.0 | 10.1 | 0.8 | 22.0 | **20.1** | **11.9** | 3.6 | 16.5 |
| 2 | 0.2 | 9.2 | 0.4 | 0.9 | 0 | 1.8 | –1.3 | 7.3 | 0.5 | 2.8 |
| 3 | 0.3 | 0.0 | 1.5 | 3.7 | –0.4 | 1.8 | –2.7 | –1.8 | 0.4 | 2.8 |
| 4 | 0.5 | 0.0 | 0.7 | –2.8 | –0.5 | 1.8 | 0.9 | 0.9 | –0.4 | –0.9 |
| 5 | 1.2 | –4.6 | –1.4 | –5.5 | –0.5 | –2.8 | **–15.0** | **–6.4** | –0.9 | –2.8 |
| 6 | –0.2 | –9.2 | –2.0 | –18.3 | 3.1 | –7.3 | 0.3 | –11.0 | **20.1** | **–20.2** |
| 7 | –0.9 | –3.7 | 1.2 | –8.3 | 1.1 | –8.3 | 0.3 | –4.6 | 0.6 | –10.1 |
| 8 | –0.5 | 3.7 | –1.9 | –1.8 | –1.3 | 4.6 | 1.4 | –0.9 | –2.1 | –0.9 |
| 9 | –1.5 | 1.8 | –1.6 | 0.9 | 0.3 | 0.9 | 0.2 | 3.7 | 0.1 | 1.8 |
| 10 | 1.2 | 3.7 | –2.1 | 6.4 | 2.9 | 6.4 | –1.3 | 0.0 | **–15.0** | **7.3** |
| 11 | –0.3 | –14.7 | **–13.8** | **–6.4** | **23.3** | **–11.0** | 2.2 | –3.7 | 1.4 | –4.6 |

## 4.2 Electronic Properties

Figure 3 shows the predicted Mulliken[22] charges for SiC Σ9 {122} polar-Si rich, polar-C rich, and nonpolar grain boundaries. Due to the delocalized nature of the CASTEP PW basis sets, the localization of the electrons in the system cannot be determined. Therefore as an approximation, CASTEP projects the PW states onto a localized basis using a technique described by Sanchez-Portal et al.[23] The predicted charge from the Mulliken equations is dependent on the basis set and therefore the magnitude of the Mulliken charges has no physical meaning. However, relative changes in the Mulliken charges can provide insight into the charge redistribution within the structure. The Mulliken analysis reveals that the effective charge for the wrong bonds within the polar Si-rich, polar C-rich, and nonpolar SiC Σ9 {122} SiC-3C grain boundaries are 70.7%, 72.5%, and 74%, respectively, of the charge assigned to C and Si in the bulk region.

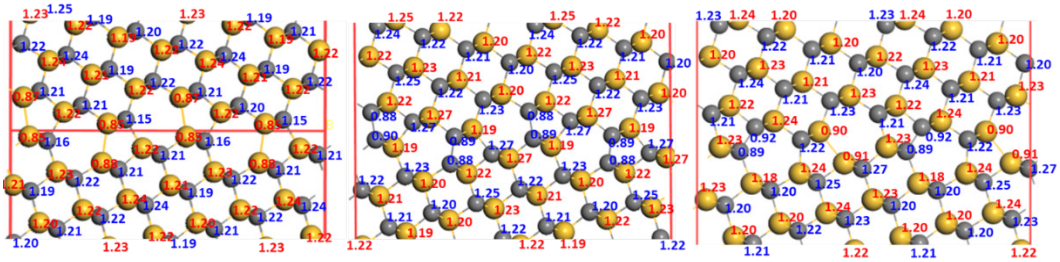

a) b) c)

**Fig. 3 Mulliken charges for SiC Σ9 {122} a) polar Si-rich, b) polar C-rich, and c) nonpolar grain boundaries**

Another powerful tool for analyzing the relationship between bond formation and electron redistribution are the EDD maps shown in Fig. 4. The EDD map plots the difference between the electron density of the optimized grain boundary and the electron density for the isolated atoms that compose the grain boundary. Specifically, it measures the changes in the electron distribution due to the delocalization of atomic charge density and the formation of chemical bonds. Figure 4 clearly shows that in the bulk-like region, chemical bonding occurs via the transfer of electrons from carbon to silicon, suggestive of mixed covalent-ionic bonding. The C-C wrong bonds in the nonpolar structure also show ionic behavior. However, there does not appear to be any significant charge transfer for C-C wrong bonds in the polar reconstruction. More charge transfer occurs to the Si-Si wrong bonds in both the nonpolar and polar SiC Σ9 {122} than occurs for the corresponding Si-Si bonds in Si Σ9 {122}.

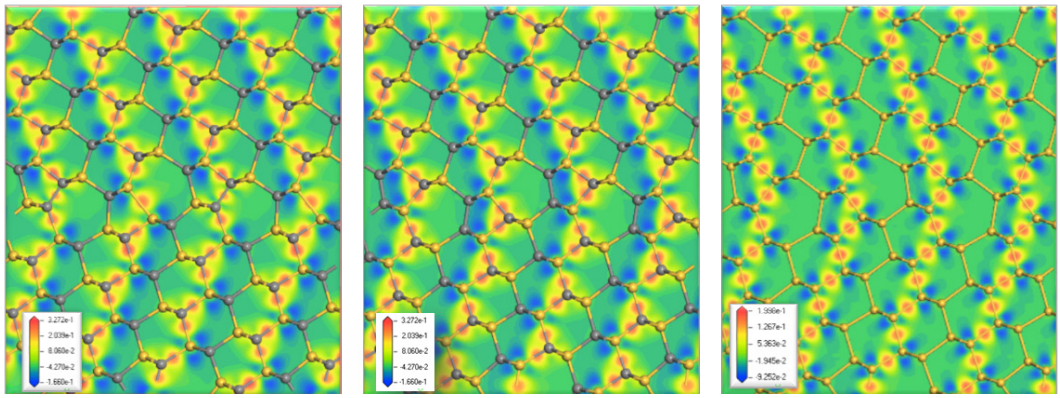

a) b) c)

**Fig. 4 EDD maps at isovalue = 0.5 for Σ9 grain boundaries a) SiC-3C nonpolar reconstruction, b) SiC-3C polar reconstruction, and c) silicon**

Figure 5 shows the atom resolved partial density of states (PDOS) for each atom comprising the structural units of SiC Σ9 {122} polar-C rich, polar-Si rich, and nonpolar grain boundaries. All three interfaces have a distinct band gap with no

energy states within the bandgap. This is consistent with a lack of dangling bonds at the grain boundary interface. An analysis of the PDOS shows significant electron populations at the Fermi level for the C-C and Si-Si wrong bonds within the polar C-rich and nonpolar structural units, suggesting that these grain boundaries are conducting. In contrast, there are no electrons near the Fermi level for all atoms comprising the structural unit of the polar Si-rich grain boundary.

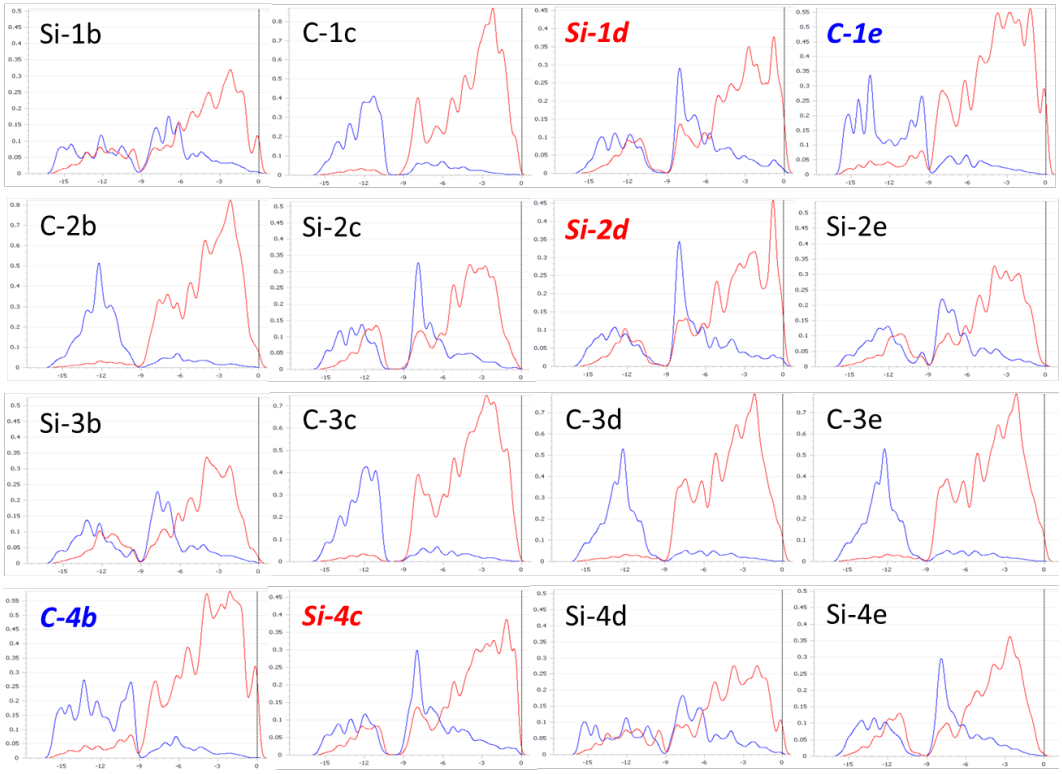


**Fig. 5 Atom resolved PDOS for each atom comprising the structural units of the SiC Σ9 {122} polar C-rich, polar Si-rich, and nonpolar grain boundaries. s- and p- orbitals are blue and red, respectively. The first letters of the label identify whether the atom was carbon or silicon. The number followed by letter refers to the position of the atom and the structural unit to which it belongs (b = polar C-rich; c = polar Si-rich; and d, e = nonpolar fragments) according to the naming convention from Fig. 1 and Table 2. For clarity, atoms associated with Si-Si and C-C wrong bonds have red and blue labels, respectively.**

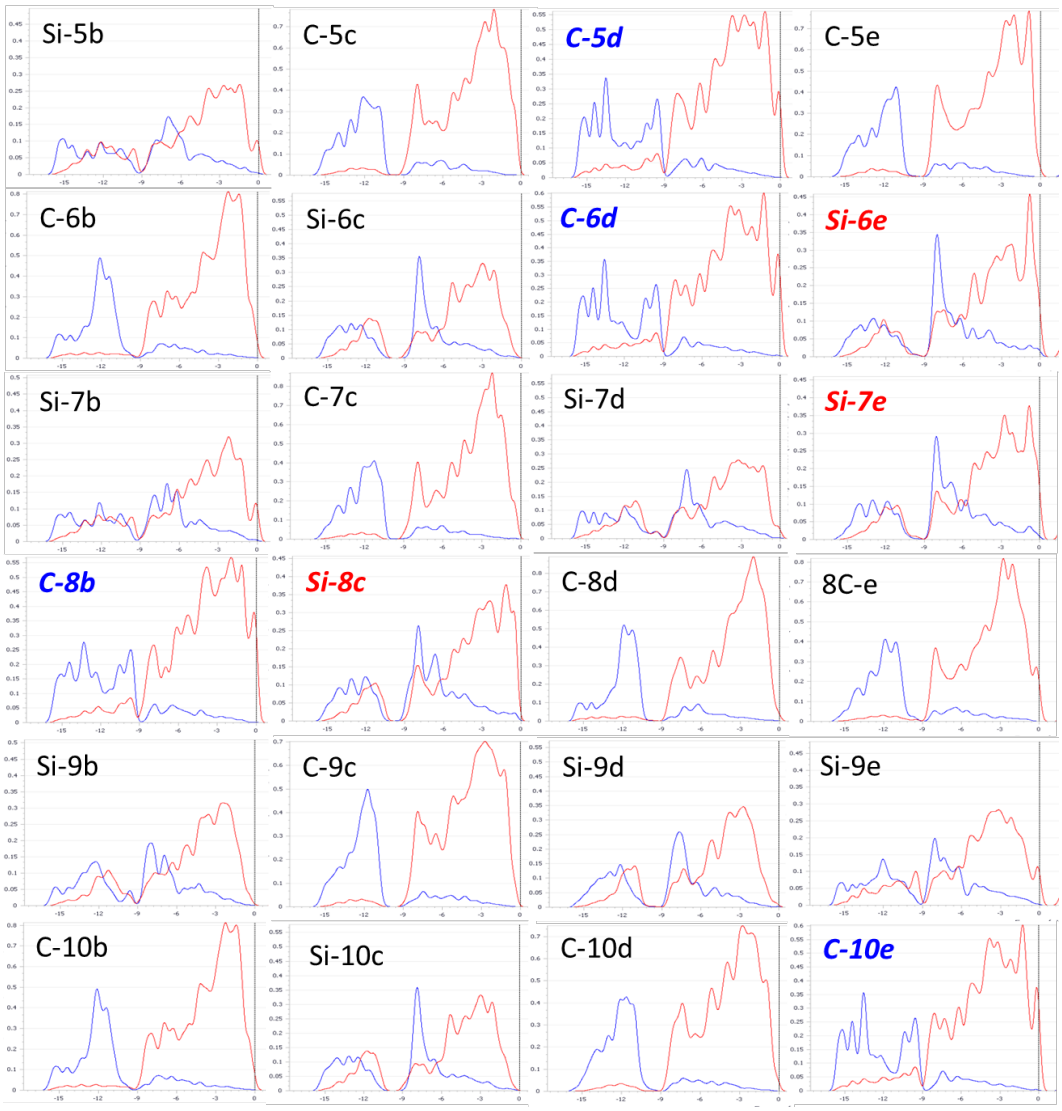


**Fig. 5 Atom resolved PDOS for each atom comprising the structural units of the SiC Σ9 {122} polar C-rich, polar Si-rich, and nonpolar grain boundaries. S- and p- orbitals are blue and red, respectively. The first letters of the label identify whether the atom was carbon or silicon. The number followed by letter refers to the position of the atom and the structural unit to which it belongs (b = polar C-rich, c = polar Si-rich; and d, e = nonpolar fragments) according to the naming convention from Fig. 1 and Table 2. For clarity, atoms associated with Si-Si and C-C wrong bonds have red and blue labels, respectively (continued).**

The PDOS for the C-C wrong bonds are identical for both the polar and nonpolar structural units. The lower valence band ([LVB], bandwidth = 7.3 eV) consists of seven peaks at –15, –14.4, –13.3, –12.3, –11.3, –10.5, and –9.6 eV with primarily s-character, whereas the upper valence band ([UVB], bandwidth = 9.6 eV) is dominated by p-orbitals at –7.9, –6.1, –5.3, –3.8, –2.7, –2, –1.1, and –0.2 eV. The LVB (bandwidth = 6–6.8 eV) for the Si-Si wrong bonds in the nonpolar structural units consists of four peaks at –14, –13, –11.8, and –11.1 with s and p character,

whereas the UVB (bandwidth = 9.65–9.85 eV) is dominated by s orbitals at –8.0, –6.9 and p orbitals at –6.1, –5.7, –5.1, –4.1, –2.7, –2.1, and –0.8 eV. The PDOS for the Si-Si wrong bonds in the polar-Si rich grain boundary are nearly identical to the PDOS for nonpolar Si-Si wrong bonds with the exception that the UVB is shifted to lower energy, making the polar Si-rich grain boundary nonconducting as previously noted.

## 5. Conclusions

The calculated grain boundary energies for the Σ9 {122} silicon, Σ9 {122} SiC-3C nonpolar, and Σ9 {122} SiC-3C polar interfaces are 0.1821, 1.346 and 1.336 J/m$^2$, respectively. Although the predicted grain boundary energy for the polar grain boundary is the average of the Si-rich and C-rich interfaces, DFT calculations show that it is more stable than the nonpolar interface in SiC-3C and therefore predicted to be slightly more prevalent throughout the SiC-3C microstructure. The reconstruction of the interface with 7- and 5- member rings containing contracted C-C and expanded Si-Si wrong bonds creates periodic compressive and tensile strain fields along the grain boundary interface that can serve as gettering sites for dopants. An analysis of the lattice distortions suggests that the grain boundary energy in the polar C-rich interface can be minimized by substituting carbon atoms with larger atomic species. Conversely, the Si-rich polar interface has a higher potential for strain energy minimization when silicon atoms are replaced by dopants with a smaller radius. In addition, it may be possible to improve lattice matching between Σ9 {122} SiC-3C boundaries and diamond by increasing the number of C-C wrong bonds.

## 6. References


1. Medvedovski E. Ballistic performance of armour ceramics: influence of design and structure. Ceram Int. 2010;36:2103–2115.

2. Neshpor VC, Zaitsev GP, Dovgal EJ. Armour ceramics ballistic efficiency evaluation. In: Vincenzini P, editor. Ceramics: charting the future. Proceedings of the 8th CIMTEC; 1994 June 38–July 2; Florence, Italy. Faenza (Italy): Techna srl; c1995. p. 2395–2401.

3. Ritchie RO. The conflicts between strength and toughness. Nat Mater. 2011;10:817–822.

4. Voigt A, Wolf E, Strunk HP. Grain orientation and grain boundaries in cast multicrystalline silicon. Mater Sci Eng B. 1998;54(3):202–206.

5. Stoffers A, Ziebarth B, Barthel J, Cojocaru-Mirédin O, Elsässer C, and Raabe D. Complex nanotwin substructure of an asymmetric Σ9 tilt grain boundary in silicon polycrystal. Phys Rev Lett. 2015;115:235502.

6. Arroyo Rojas Dasilva Y, Erni R, Isa F, Isella G, von Känel H, Gröning P, Rossell MD. Atomic-scale structural characterization of grain boundaries in epitaxial Ge/Si microcrystals by HAADF-STEM. Acta Materialia. 2019;167:159–166.

7. Chang L, Chen FR. Interfacial structure of a Σ9 and defect structure at the junctions of Σ3 Σ9 Σ3 in diamond film. Mater Sci Forum. 1995;189.

8. Kohyama M, Tanaka K, Tanaka S. First principles study of a {122} = 9 boundary in cubic SiC: relative stability between zigzag and straight models and comparison with electron microscopy observation. Mater Trans. 2004;45(5):1461–1464.

9. Kohler C. Atomistic modelling of structures of tilt grain boundaries and antiphase boundaries in beta silicon carbide. Phys Stat Sol. 2002;234(2):522–540.

10. Banadaki AD, Tschopp M, Patala S. An efficient Monte Carlo algorithm for determining the minimum energy structures of metallic grain boundaries. Comp Mat Sci. 2018;155:466–475.

11. Tersoff J. Modeling solid-state chemistry: interatomic potentials for multicomponent systems. Phys Rev B. 1989;39:5566(R).

12. Plimpton S. Fast parallel algorithms for short-range molecular dynamics. J Comp Phys. 1995;117:1–19.

13. LAMMPS molecular dynamics simulator. Albuquerque (NM): Sandia National Laboratories [accessed 2015 Oct 10]. https://lammps.sandia.gov/index.html.

14. Clark SJ, Segall M, Pickard C, Hasnip P, Probert M, Refson K, Payne M. First principles methods using CASTEP. Zeitschrift fuer Kristallographie. 2005;220(5–6):567–570.

15. Perdew JP, Burke K, Ernzerhof M. Generalized gradient approximation made simple. Phys Rev Lett. 1996;77:3865.

16. Vanderbilt D. Soft self-consistent pseudopotentials in a generalized eigenvalue formalism. Phys Rev B. 1990;41:7892–7895.

17. Presser V, Nickel KG. Silica on silicon carbide. Crit Rev Solid State Mater Sci. 2008;33(1):1–99.

18. Okada Y, Tokumaru Y. Precise determination of lattice parameter and thermal expansion coefficient of silicon between 300 and 1500K. J App Phys. 1984;56:314–320.

19. Atkinson C, Guziewski M, Coleman S. Density functional theory study of the impact of defects in silicon carbide bulk and grain boundaries. Aberdeen Proving Ground (MD): CCDC Army Research Laboratory; 2019 Oct. Report No.: ARL-TR-8836.

20. Ziebarth B, Mrovec M, Elsässer M, Gumbsch P. Interstitial iron impurities at grain boundaries in silicon: a first-principles study. Phys Rev B. 2015;91:035309:1–7.

21. Zhao D, Li Y. Revealing the factors influencing grain boundary segregation of P, As, in Si: insights from first principles. Acta Materialia. 2019;168:52–62.

22. Mulliken RS. Electronic population analysis on LCAO–MO molecular wave functions. J Chem Phys. 1955;23:1833–1846.

23. Sanchez-Portal D, Artacho E, Soler JM. Projection of plane-wave calculations into atomic orbitals. Solid State Commun. 1995;95:685–690.

## List of Symbols, Abbreviations, and Acronyms

| | |
|---|---|
| ARL | Army Research Laboratory |
| BA | bond angle |
| BL | bond length |
| CCDC | US Army Combat Capabilities Development Command |
| DFT | density functional theory |
| EDD | electron density difference |
| GGA | generalized gradient approximation |
| LAMMPS | Large-scale Atomic/Molecular Massively Parallel Simulator |
| LVB | lower valence band |
| PDOS | partial density of states |
| PW | plane wave |
| UVB | upper valence band |

| | |
|---|---|
| 1 (PDF) | DEFENSE TECHNICAL INFORMATION CTR DTIC OCA |
| 1 (PDF) | CCDC ARL FCDD RLD DCI TECH LIB |
| 3 (PDF) | CCDC ARL FCDD RLW ME S COLEMAN M GUZIEWSKI J SYNOWCZYNSKI-DUNN |